Open Ceramics 16 (2023) 100458

Contents lists available at ScienceDirect

Open Ceramics

journal homepage: www.sciencedirect.com/journal/open-ceramics

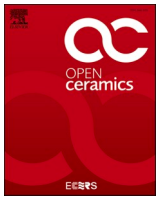

Steel ceramic composite anodes based on recycled MgO–C lining bricks for applications in cryolite/aluminum melts

S. Yaroshevskyi [a,*], C. Weigelt [a], P. Malczyk [a], V. Roungos [a], J. Hubalkova [a], T. Zienert [a], B. Kraft [b], S. Wagner [b], C.G. Aneziris [a]

[a] Institute of Ceramics, Refractories and Composites, TU Bergakademie Freiberg, Agricolastr. 17, 09599, Freiberg, Germany
[b] Germany Institute for Applied Materials - Ceramic Materials and Technologies, Karlsruhe Institute of Technology, Haid-und-Neu-Straße 7, 76131, Karlsruhe, Germany

ARTICLE INFO

Keywords:
Recycling
Upcycling
Inert anode
Cryolite
Aluminium
MgO
Steel ceramic composite

ABSTRACT

Novel manufacturing route for composite inert anodes containing 60:40 of 316 L stainless steel and MgO powder obtained from recycled MgO–C brick material has been developed and evaluated. After burnout of residual carbon from the recycled MgO–C powder, MgO and steel were granulated and pre-sintered in order to generate agglomerates of composite material acting as coarse grains within the composite material, and thus lowering the sintering-related shrinkage. The pre-sintered granules were mixed with raw steel and MgO powder in order to achieve a high particle packing and subsequently cold isostatically pressed in the form of electrodes. All manufactured anode samples were subjected to sintering at 1350 °C and pre-oxidation at different temperatures – 800 °C, 900 °C, and 1000 °C. Afterwards, mechanical and electrical properties of the manufactured electrodes were characterized. The results show that upcycling of the MgO–C material enables manufacturing of sophisticated electrode products, which can be applied in the aluminum industry.

1. Introduction

Refractories are commonly used in high-temperature applications such as production of metal, cement, glass, and ceramics. Despite significant amounts of refractory materials being used every year, recycling of such products gained attention only in the recent years. In 2019 recycling rate for refractories was estimated to be only 7% of raw material demand by Horkmans et al. [1]. Bittencourt expects recycling rate of refractory materials to have increased up to 10% by 2025 [2]. Apart from the energy prices, production costs of refractory materials rise every year. Moreover, necessity of environmental protection is becoming more and more obvious [3]. Besides recycling of the refractory materials, another possible way to decrease disposal rate of refractories is to utilize the materials ones that came to the end of their life cycle, is to produce more profound and complicated functional parts, specifically, upcycle the refractories.

In metal industry, the largest part of refractories is dolomite, followed by magnesite, fireclay and bauxite [3]. MgO–C lining bricks have been gaining more and more attention over recent decades and nowadays they are widely used in basic oxygen furnaces, electric arc furnaces, and steel ladle furnaces due to their excellent resistance to thermal shock, slag penetration, and corrosion; i.e. their outstanding properties at elevated temperature [4–7]. Global demand for refractory materials was estimated in 46 million tons for 2016, around 65% of which is consumed by steel industry. Klages et al. estimated that around 40% of the original converter lining is wearing out, and approximately 50% of the remaining material is recyclable refractory material [8]. It ends up in around 9–10 million tons of recycled refractories per year. Such materials might be used for land refilling or recycling. European commission included waste framework directive 2008/98/EC outlining the priority order for waste management as follows: A) Prevention, B) Reuse, C) Recycling, D) Recovery, E) Disposal [1]. On the way to Zero waste policy within industries it is important to use spent materials for recycling, which will also prevent environmental problems caused by landfill and toxic materials. According to Moritz et al., MgO–C bricks that contain recyclate perform similarly good in comparison with the conventional MgO–C bricks in terms of thermal shock resistance, even with a content of recyclates up to 80% by mass [9]. However, due to decrease in CMOR and RUL while containing a high ratio of recyclate, such material could be suitable for applications with relatively low refractory requirements [9]. Among the application fields of MgO-containing materials that do not require outstanding refractoriness, there are composite materials

* Corresponding author.
E-mail address: serhii.yaroshevskyi@ikfvw.tu-freiberg.de (S. Yaroshevskyi).

https://doi.org/10.1016/j.oceram.2023.100458
Received 14 July 2023; Received in revised form 4 September 2023; Accepted 4 September 2023
Available online 6 September 2023

Table 1
Chemical composition of the 316 L stainless steel in wt.%.

Element	Fe	Cr	Ni	Si	Mo	Mn	Ti	Nb	S	Al
	Balance	16.9	10.5	0.1	2.1	0.9	<0.001	0.02	0.01	0.07

applicable: in field of plasma resistance for semiconductors application [10], and in field of corrosion resistance against molten aluminium alloys. According to Malczyk et al., steel-ceramic composite comprising of 316 L stainless steel and of MgO powder exhibited outstanding corrosion resistance against molten aluminium alloys after particular thermal treatment [11], due to the formation of MgO–FeO solid solution on their surface [12]. Weigelt et al. showed that composite based on 316 L steel and MgO is resistant to molten cryolite [13]. Thus, it might be possible to utilize spent MgO–C brick material for aluminium production (where corrosion resistance is of more importance than refractoriness of the material), e.g. as inert electrodes for the alumina-cryolite electrolytic cell process.

Haggerty et al. fundamentally investigated materials for inert electrodes in aluminum electrodeposition cells [14]. There are few metal oxides which do not co-deposit in the aluminum by electrochemical deposition or chemical displacement, such as: MgO, SrO, La_2O_3, CaO. However, such oxides have a significant solubility in cryolite. Therefore, Haggerty et al. labelled MgO among other materials as “not of great interest on anode formulations to date” [14]. Nowadays, most commonly used electrodes for production of aluminum-silicon alloys in cryolitic melts are consumable graphite anodes [15]. Galasiu and Thonstad gave a comprehensive overview of inert anodes for electrowinning of aluminium [16], dividing them into three categories.

1. Ceramic inert anodes, especially based on SnO_2 doped with CuO and Sb_2O_3, being prepared from oxides and therefore not oxidizing during electrolysis.
2. Cermet inert anodes combining two different phases: ceramic phase which is resistant to oxidation, however lacks electrical conductivity; and metallic phase added to increase the electrical conductivity. The major disadvantage of such materials is the oxidation of the metallic part during the electrolysis process.
3. Metallic inert anodes utilizing specific alloys that undergo a surface oxidation during electrolysis, forming oxide layers with low solubility in the electrolyte. The surface layer of such electrodes has to be electrically conductive and impermeable to oxygen.

There is an increasing argument that the introduction of inert anodes would have a little to none environmental benefits due to higher DC energy consumption with inert anodes [17,18]. However, Kargin et al. [19] and Zhang et al. [20] studied metal ceramic composites, mostly based on Fe–Ni, Cu–Ni–Fe, Fe–Ni–Al alloys. Yang et al. showed that inert anodes based on metal-ceramic composite with $NiFe_2O_4$ spinel exhibit excellent corrosion resistance paired with self-repairing behavior under oxidation atmosphere [21].

It must be noted that fine-grained metal ceramic composites suffer from the high shrinkage during sintering process, which drastically limits dimensions of the manufactured body. A concept of coarse-grained composite materials (manufacturing and pre-sintering aggregates of desired size from fine powders) was recently introduced [22]. The sintered aggregates have already experienced shrinkage during pre-sintering process. Therefore, after mixing with fine powders to form a dense body, they will significantly decrease shrinkage of the manufactured composite material [23].

This research focuses on the utilization of the recycled MgO–C lining bricks to manufacture cermet inert composite anodes for the aluminium cryolite electrolytic cells. Furthermore, this research studies implementation of the novel manufacturing process, i.e. pre-sintering of aggregates of composite materials in order to decrease the sintering-related shrinkage of the products. The manufactured electrode samples were characterized of regarding E-modulus, splitting tensile strength, electrical conductivity at room temperature, as well as microstructure.

Table 2
Manufacturing route of the composite granulate.

	Material addition	Mixing/granulating parameters
Step 1	Adding raw powders	Dry mixing for 120 s at 300 min^{-1}
Step 2	Adding 1 wt% of de-ionized water	Mixing for 60 s at 300 min^{-1}
Steps 3–9	[Adding 1 wt% of binder material	Mixing for 60 s at 300 min-1] ×7 times
Step 10	–	Granulating for 100 s at 600 min^{-1}

2. Methods and materials

2.1. Materials

Crushed MgO–C bricks were provided by Refratechnik Steel GmbH with particle size of 0–1 mm. For the manufacturing of the anode samples as well as for the granulate production, the finest MgO–C fraction – less than 125 μm – was sieved out and only this fraction was used throughout the whole research. Carbon content of the powder was estimated to be approximately 19.3 wt% by means of the oxidation test: Nabertherm LHT 04/16 S W oven (Nabertherm GmbH, Lilienthal/Bremen, Germany) is equipped with weigh that allows to continuously measure mass of the sample during the heating process to desired temperature. 12.5 g of the sieved fine fraction of MgO–C material were slowly heated up with heating rate of 2.5 K/min until mass of the sample stabilizes (approximately 6.5 h, reaching 950 °C). Therefore, 24 h at 1000 °C was chosen as the sufficient thermal treatment to burn out all the residual carbon (conducted in Nabertherm N 20/14 ventilated oven under air). The true density of MgO powder was estimated with 3.58 g/cm^3, particle size d90 < 109 μm.

The steel powder of gas-atomized 316 L-FeCr18Ni10Mo3 stainless steel (TLS Technik, Bitterfeld-Wolfen, Germany) was used as a metallic part for metal ceramic composite. Chemical composition of the steel is provided in Table 1. True density of the 316 L stainless steel is 7.62 g/cm^3, particle size d90 < 51 μm.

Carbonless recyclate powder was then used to produce steel-ceramic composite material with volumetric ratio 60 vol% 316 L stainless steel powder +40 vol% carbonless MgO recyclate powder. For the coarse-grain aggregates manufacturing, granulation process was chosen. Binder material for the granulation process was water solution of the fructose syrup 70% (Gellmi, Hanseatische Zuckerraffinerie, Hamburg, Deutschland) in proportion 30 wt% fructose syrup to 70 wt% deionized water. Fructose was chosen as environmentally friendly binder material following the sustainability and upcycling concepts of the Research Training Group GRK 2802.

2.2. Aggregates manufacturing

Laboratory mixer Eirich EL-1 (Maschinenfabrik Gustav Eirich, Hardheim) was used to mix and to granulate thw powders of carbonless MgO-recyclate, 316 L stainless steel, water and binder material. Granulation process is described in detail in Table 2.

After the granulation, the material was dried at 110 °C for 24 h, with further debinding at 500 °C under air atmosphere for 30 min in Xerion Entbinder-und Sinter Sonderofen (XERION ADVANCED HEATING

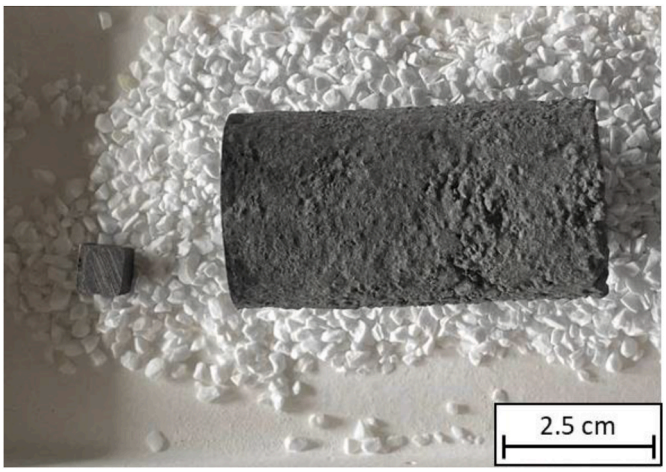

Fig. 1. Photograph of specimens prior to oxidation used for electrical conductivity measurement (left) and for tensile spitting test (right).

Ofentechnik GmbH, Freiberg, Germany). Parameters of the debinding process were: heating rate 2 K/min to 200 °C, 0.5 K/min to 500 °C and cooling rate 0.5 K/min to 100 °C. After debinding, material was directly transferred to sintering furnace Xerion XGRAPHIT Hochtemperatur-Vakuum-Ofensystem (XERION ADVANCED HEATING Ofentechnik GmbH, Freiberg, Germany), and sintered at 1350 °C for 2 h. Sintering was conducted under argon atmosphere with heating rate 5 K/min to 1350 °C, cooling rate 5 K/min to 300 °C followed by free cooling to room temperature.

Pre-sintered granulates of composite material were fractioned by means of sieves with mesh-sizes 8 mm, 6.3 mm, 3.15 mm, 2 mm, 1 mm, 500 μm, and 250 μm. Small amount of sintered granulate material was embedded in epoxide and polished in order to conduct XRD analysis. Results for granulate containing carbonless MgO were then compared to the results of XRD analysis of granulate prepared with conventional fused MgO powder (Refratechnik GmbH, d90 < 100 μm).

2.3. Electrodes manufacturing and testing

After sieving, the pre-sintered granulate material was split into three fractions, coarse particles in range 2–6.3 mm, medium grains in range 0.5–2 mm, and fines containing mixture of 316 L stainless steel powder with carbonless MgO recyclate powder in a respective volumetric ratio 60:40. Mass ratio coarse:medium:fines was chosen to be 2:1:2 in order to achieve a high packing density and thus to compact the composite material during pressing. As a pressing aid, Zusoplast G63 (Zschimmer & Schwarz GmbH & Co KG Chemische Fabriken, Lahnstein, Germany) in an amount of 0.5 wt% of the material mixture was added. The composite material was pressed in a latex mould (with a diameter of 35 mm and a height of 155 mm) with a 150 MPa pressure using cold isostatic press EPSI CIP 300–250 × 1000 Y (Engineered Pressure Systems International NV, Temse, Belgium). After the CIP pressing, the compacts were subjected to the same debinding and sintering procedures as granulated composite material.

The sintered compacts were cut in four cylindrical specimens with a height of 70 mm and a diameter of about 35 mm (depending on the diameter of the parts after pressing) (Fig. 1). The cylindrical specimens were used for E-modulus acoustic measurement with UltraTest Ultrasonic Tester BP-700 (UltraTest GmbH, Achim, Germany). After non-destructive E-modulus testing, three specimens were pre-oxidized at 800°C, 900°C, and 1000°C and used for acoustic E-modulus test again. Afterwards, one specimen in as-sintered state (reference) and three pre-oxidized specimens were tested for tensile splitting strength using Toni Technik 40–4000 kN testing machine (Toni Technik Baustoffprüfsysteme, Berlin, Germany) with speed of 0.06 N/mm^2/s according to DIN EN 12390–6.

For electrical conductivity measurement, four prisms with dimension of 8 mm in height and 9 mm × 9 mm in cross-section were cut from the sintered electrode samples. A set of four prisms was prepared in the same way – reference prism in as-sintered state and the three other prisms pre-oxidized at 800 °C, 900 °C, and 1000 °C. Before electrical conductivity measurement, the surface of the specimens was sputter coated with a layer of gold using Quorum Q150T ES. To reduce the influence of surface roughness and to ensure a continuous contacting over the whole sample surface, an additional layer of Pelco Colloidal Silver (Plano GmbH, Wetzlar, Germany) was applied. Electrical conductivity was measured with a Keithley 220 Programmable Current Source (Keithley Instruments, Cleveland, OH, USA) and a Keithley 2000 Multimeter (Keithley Instruments, Cleveland, OH, USA) using four-point-measurement setup by applying electrical currents of 1 mA, 10 mA, and 100 mA and measuring the resulting voltages.

Due to the fact that new MgO–FeO phases are formed on the surface of the specimens during pre-oxidation, the grinding or polishing of the surface should be avoided.

Another set of four disks with a height of 8 mm were cut from the sintered electrode. Three of the disks were pre-oxidized at 800 °C, 900 °C, and 1000 °C, the fourth served as a reference (as-sintered state). Afterwards, all four disks were cut in half, embedded into epoxide and vibro-polished for REM/EDS analyses in order to estimate surface oxidation depth and rate.

3. Results and discussion

3.1. Aggregates manufacturing

All preliminary burnout treatment tests of recycled MgO–C material were conducted with thickness of MgO–C layer below 10 mm. However, taking into consideration high amount of the material needed to produce the electrodes, the first campaign was carried out with a larger thickness of approx. 35 mm. After pre-sintering of the granulates based on this material at 1350 °C under argon atmosphere, it was found that the residual carbon from the recyclate material led to the carburization of the stainless steel, hence, lowering its melting point. Droplets of the molten steel could be detected at the surface of such granulates (Fig. 2).

Therefore, it was decided to further decrease thickness of the layer of

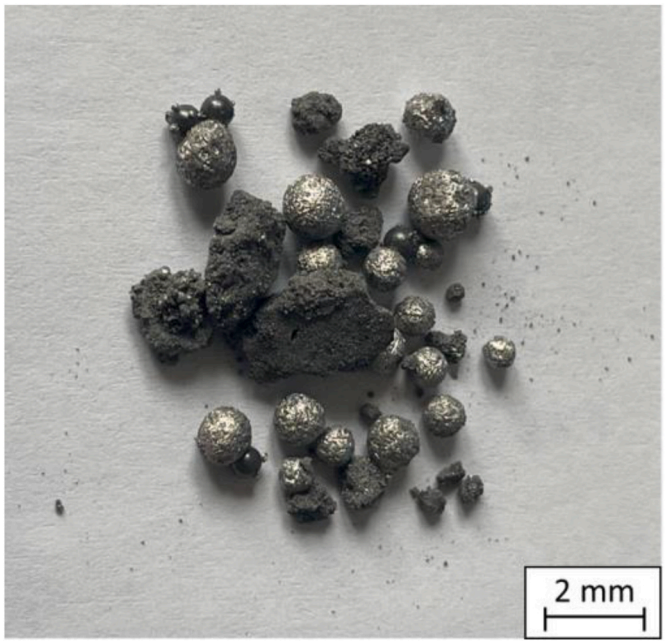

Fig. 2. Steel droplets formed due to carburization of 316 L stainless steel.

Fig. 3. Pre-sintered granulates with 60 vol% 316 L and 40 vol% carbonless MgO powder.

the material for the burnout treatment to 5 mm. Subsequent TG analysis of the material indicated no noticeable change of mass and thus no presence of carbon.

After adjustment of the manufacturing route, granulate material was produced in small batches of 800 g to prevent the formation of sintering necks. An example of pre-sintered 800 g batch can be seen in Fig. 3.

After pre-sintering, the granulate material was sieved, particle size distributions of three 800 g batches are shown in Fig. 4. Obviously, particle size distributions naturally varied from batch to batch, however common trend could be observed. Based on the particle size distribution, particles between 2 mm and 6.3 mm (marked blue in Fig. 4) were chosen as a coarse fraction, and 0.5 mm–2 mm – as medium (marked orange in Fig. 4) for 40:20:40 coarse:medium:fines composition, due to the fact that cumulative masses of 2 mm–6.3 mm and 0.5 mm–2 mm ranges relate in a proportion quite close to 2:1. Fines were made up of raw materials consisting of 60 vol% of 316 L stainless steel and 40 vol% of

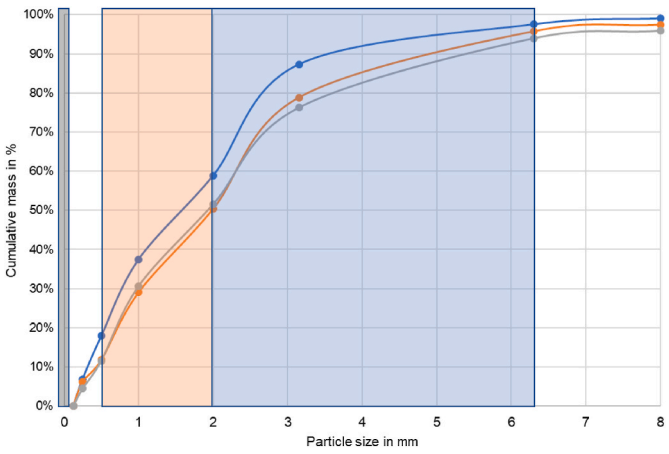

Fig. 4. Particle size distribution of three different batches of the pre-sintered granulates.

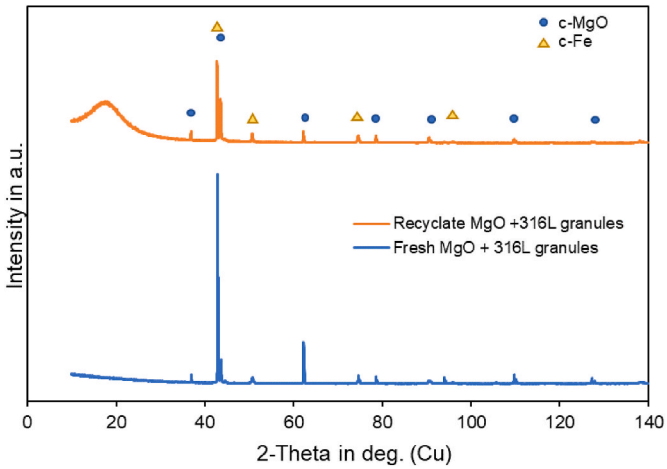

Fig. 5. XRD analysis of the pre-sintered granulates produced with carbonless MgO recyclate (top) and granulate with fused MgO (bottom).

carbonless MgO recyclate. The finest sieved fractions (<0.5 mm) were not used in order to maintain exact volumetric ratio of 316 L to MgO of 60 to 40 (see Fig. 5).

3.2. XRD analysis of the granulate

According to results of XRD analysis, both pre-sintered granulates show very similar diffraction patterns. The only difference is a broaden peak in the range of 10–25 2-θ which can be attributed to the compounds that impregnated MgO grains during metallurgical application.

3.3. Electrodes manufacturing

The dimensions of the compacts were measured after cold isostatic pressing and after sintering at 1350 °C. Due to the fact that electrode material contained granules with max size of 6.3 mm, some parts of the electrode surface featured granular texture as shown in Fig. 6. Initially it

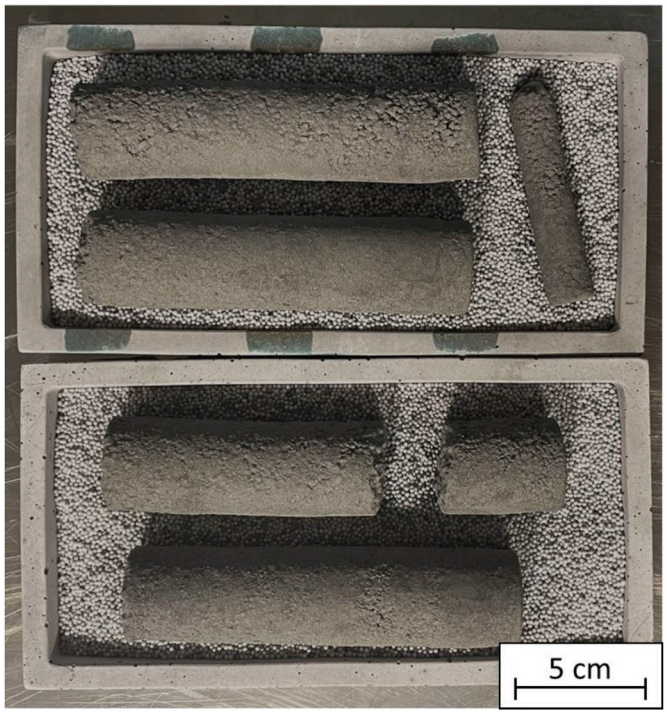

Fig. 6. Cold isostatically pressed electrode samples.

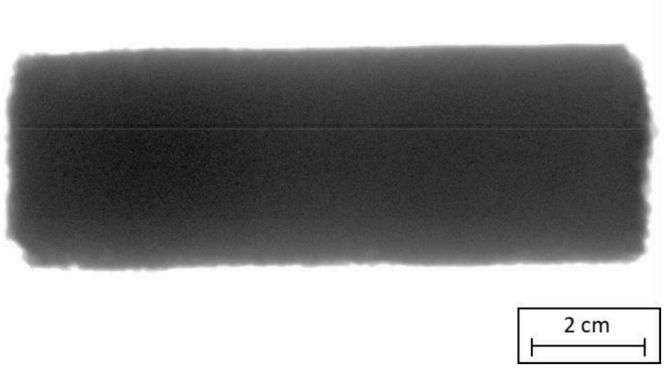

Fig. 7. X-Ray transmission image of a sintered electrode specimen.

was intended to produce electrodes with a diameter of 15 mm directly. However, the coarse grain sizes up to 6.3 mm caused an insufficient compacting, i.e. it was not possible to remove the compact from the late mould without failure.

The utilization of pre-sintered granulate in cylinder production resulted in the average sinter shrinkage of 0.75% in length and 2.14% in diameter, which is significantly lower than shrinkage of fine-grained 316 L-MgO 60–40 composite material (4%) produced by Malczyk et al. [11]. Such decrease in shrinkage was expected due to the fact that granulate of composite material, has already experienced shrinkage during pre-sintering process at the targeted 1350 °C.

After the sintering process, no visible cracks and pores could be detected, neither on the surface nor inside using X-Ray transmission imaging of the electrodes (Fig. 7).

3.4. Characterization of the electrode material

After pre-oxidation, new oxidation phases occurred on the surface of the specimens. Such phases are expected to be corrosion resistant against molten aluminium [11] as well as cryolitic melts [13]. The most important requirement is that the electrode specimens remain electrically conductive after pre-oxidation thermal treatment.

Discs for microscopical analysis, cylinders for splitting tensile strength, and prisms for electrical conductivity tests after pre-oxidation noticeably changed their appearance. Surface of the specimens that were pre-oxidized at 800 °C became darker, having no visual difference in color between them and the specimens pre-oxidized at 900 °C. On contrast, specimens pre-oxidized at 1000 °C additionally featured glassy surface (Fig. 8). After pre-oxidation thermal treatment at 800 °C, 900 °C and 1000 °C, a mass increase was determined with 0.03%, 0.16%, and 2.49% respectively. High gain of mass for 1000 °C pre-oxidized specimen indicates high rate of oxides formation, influencing both electrical conductivity and corrosion resistance of the material.

Results of acoustic E-modulus tests on the set of the same specimens before and after pre-oxidation are represented in Fig. 9. It is noticeable that E-modulus for specimens pre-oxidized at 800 °C and at 900 °C significantly increased, whereas for 1000 °C it dropped by almost 8%. Taking into consideration that only a thin surface layer is exposed to oxidation, such results may indicate that in case of 800 °C and 900 °C,

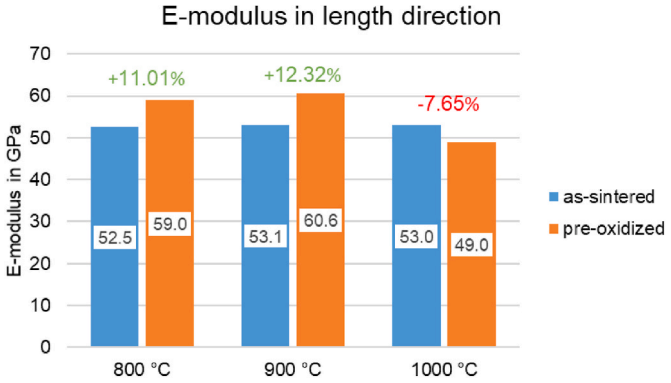

Fig. 9. Results of E-modulus acoustic measurements on cylinder specimens: before pre-oxidation (blue) and after pre-oxidation (orange). (For interpretation of the references to color in this figure legend, the reader is referred to the Web version of this article.)

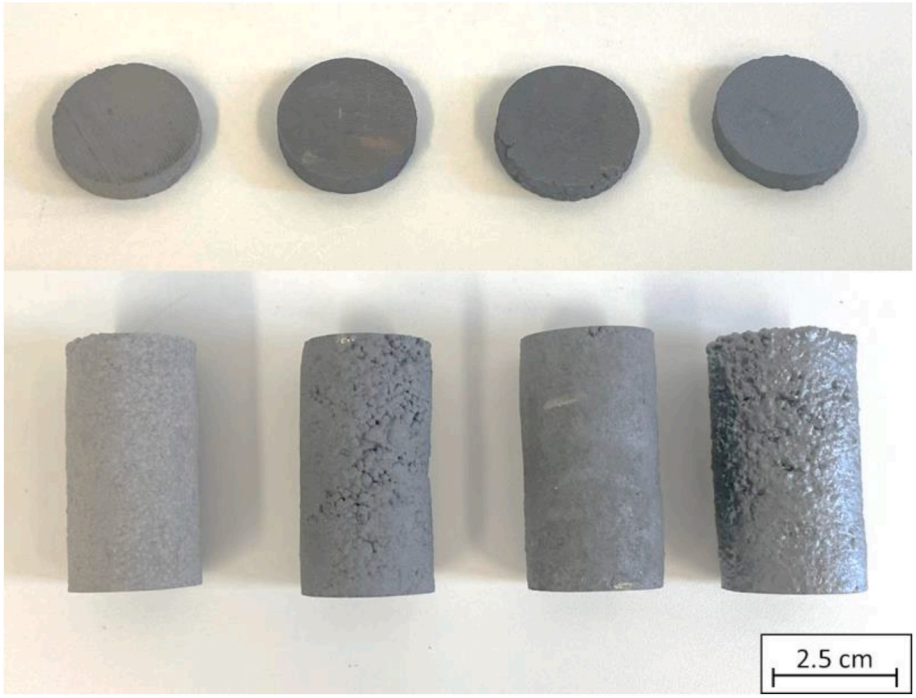

Fig. 8. Photograph of the specimens cut from the sintered electrode samples. Left to right: as-sintered, pre-oxidized at 800 °C, at 900 °C, and at 1000 °C specimens.

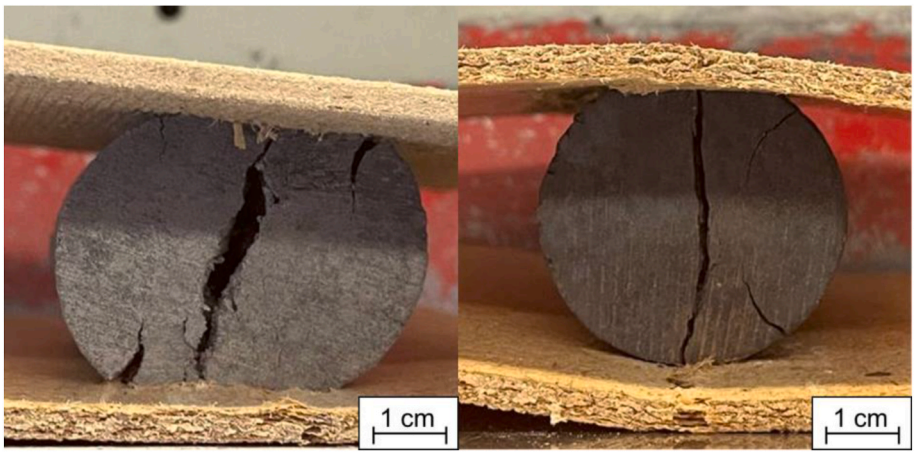

Fig. 10. Photographs of specimens after tensile splitting test, as-sintered (left) and pre-oxidized at 900 °C (right).

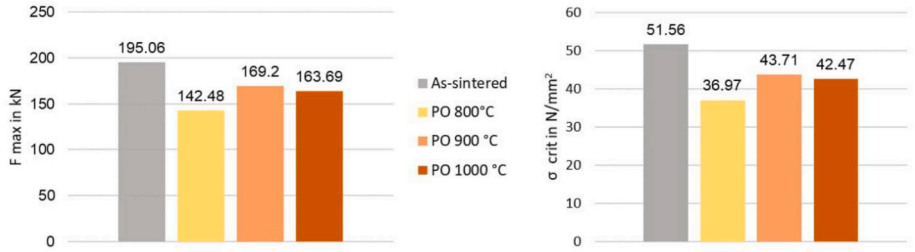

Fig. 11. Results of the tensile splitting test of samples in as-sintered state, pre-oxidized at 800 °C, 900 °C, and 1000 °C.

oxidation reaction formed stronger phases compared to 1000 °C specimen that might have experienced excessive oxidation.

After non-destructive characterization of the specimens, they were subjected to tensile splitting strength test. In order to ensure a uniform force distribution, wooden planks were used underneath and on top of the samples (Fig. 10).

It is noticeable that the as-sintered sample experienced more ductile fracture compared to the pre-oxidized sample. The thickness of the oxidation layer of the specimens pre-oxidized at 900 °C was lower than 2.5 mm, and even such thin surface layer, can affect the fracture mode. Results of splitting tensile strength test are shown in Fig. 11.

In summary, pre-oxidized specimens exhibited lower values for fracture force and critical stress, which is related to the fact that oxides newly formed on the surface of the samples are more brittle than metal matrix composite material of as-sintered samples. Specimens pre-oxidized at 900 °C performed comparatively better than specimens pre-oxidized at 800 °C or 1000 °C. Surface oxidation layer formed at 900 °C thus provides promising mechanical properties.

3.5. Electrical conductivity measurements

The electrical conductivity of specimens pre-oxidized at 1000 °C was below the sensitivity range of the measurement setup. Therefore, such specimens are considered not having sufficient electrical conductivity. On the contrary, specimens sintered and the pre-oxidized at 900 °C exhibited electrical conductivity of almost 150 S/cm at room temperature, which is comparable to electrical conductivity of carbon. Specimens pre-oxidized at 800 °C specimen showed an electrical conductivity of approx. 42.2 S/cm. As-sintered specimen exhibited electrical conductivity comparable with graphite at 985 S/cm (Fig. 12). High electrical conductivity of sintered composite material is necessary, while after pre-oxidation treatment newly formed oxide surface phases always

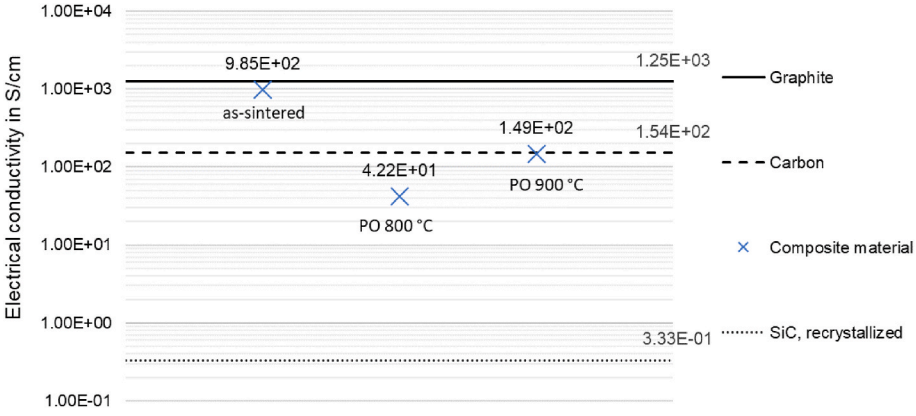

Fig. 12. Results of the electrical conductivity measurements at room temperature compared with conductivity of graphite, carbon and SiC [24].

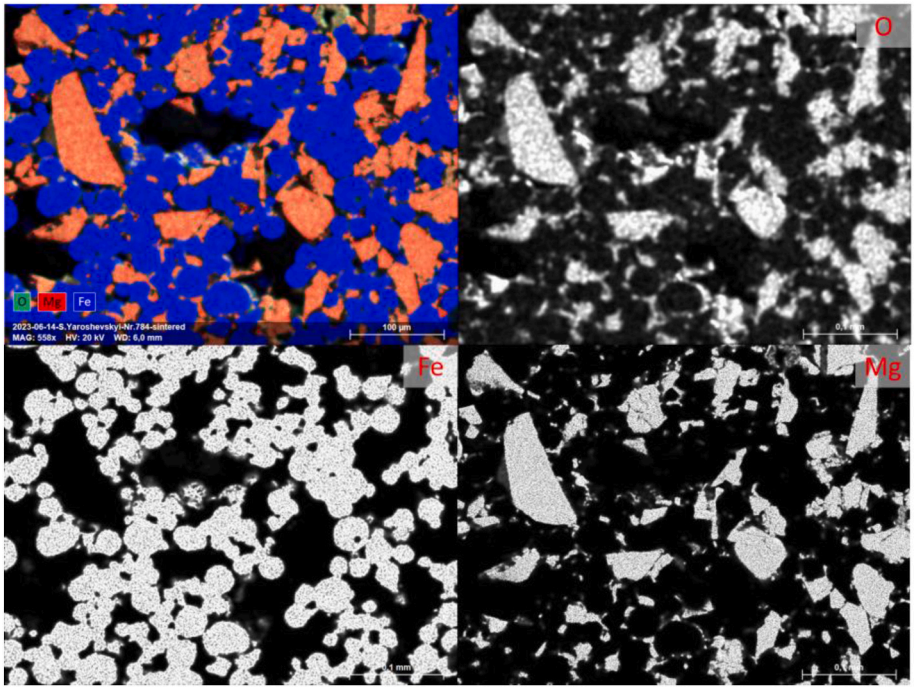

Fig. 13. EDS mapping of Mg, Fe, O elements on the surface of an as-sintered specimen.

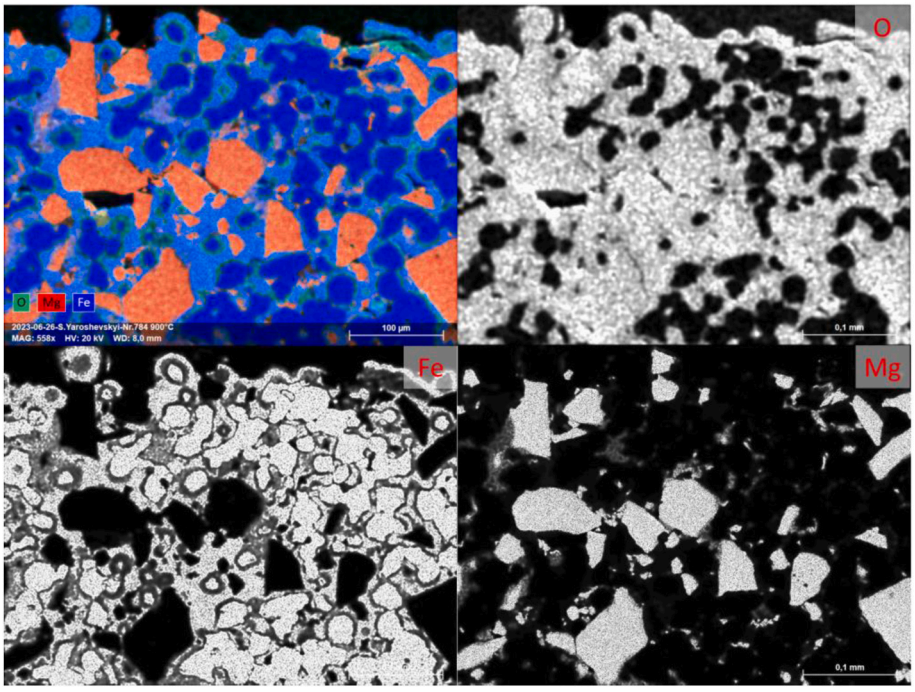

Fig. 14. EDS mapping of Mg, Fe, O elements on the surface of a specimen pre-oxidized at 800 °C.

decrease electrical conductivity of the whole part.

Adler [25] stated that the SnO_2 based anode slowly dissolves in cryolite. Doping SnO_2 with Fe_2O_3 decelerated the dissolution rate. A sample with a composition of SnO_2 with 1 wt% of Sb_2O_3 + 2 wt% of Fe_2O_3 provided an electrical conductivity of 220 S/cm [26]. The highest electrical conductivity 700 S/cm among inert anodes exhibited complex Fe-($NiFe_2O_4$ + NiO) with composition of 50 wt% NiO, 20 wt% Fe and 30 wt% $NiFe_2O_4$. However, by reducing the iron from 20 wt% to 7 wt%, electrical conductivity dropped from 700 S/cm to 19 S/cm [27–29]. In an aluminium-cryolite cell, anode is not only the electrically conductive material, but also provides heat to the melt. Therefore, it is important to adjust electrical conductivity with accordance to the application area, which will be pursued in further studies. Moreover, due to presence of the oxides in the surface layer, electrode after pre-oxidation might exhibit not only electron conductivity in composite material inside, but also partial semi-conductivity at the interface oxide-composite. At elevated temperatures, the electrical conductivity of the composite material decreases, while semi-conductivity increases. This issue will be studied in future research along with chemical inertness of the oxidized composite material against cryolite melts.

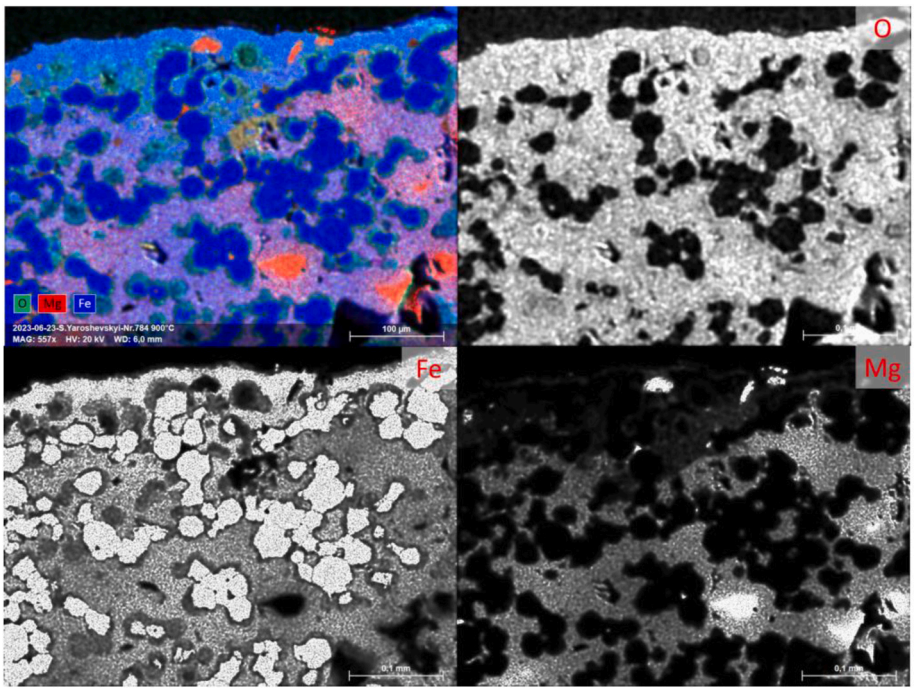

Fig. 15. EDS mapping of Mg, Fe, O elements on the surface of a specimen pre-oxidized at 900 °C.

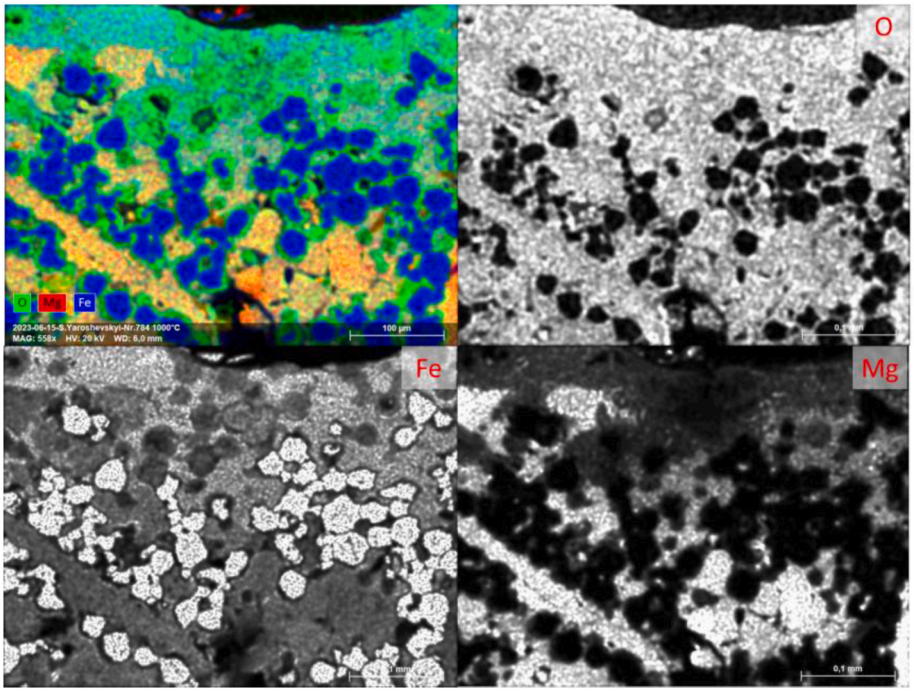

Fig. 16. EDS mapping of Mg, Fe, O elements on the surface of a specimen pre-oxidized at 1000 °C.

3.6. Microstructure analysis

According to the mapping of the Mg, Fe, O elements on the surface layer acquired with EDS-analysis, the as-sintered composite material contains MgO grains surrounded by 316 L steel with no indication of steel grains oxidation (Fig. 13). After pre-oxidation step at 800 °C, oxides of iron are formed on the surface of 316 L grains with thickness up to 40 μm, Mg is present only in very low amount within such phases (Fig. 14). After pre-oxidation at 900 °C, new phases including Fe, Mg and O are formed around former MgO grains. Concurrently, a sufficient amount of 316 L steel grains is present in order to form the continuous phase of conductive material. On the outer surface of the discs, a thin layer of iron oxides is formed (Fig. 15). At 1000 °C, the oxidation of the outer layer is excessive, almost all MgO grains reacted with Fe from 316 L grains forming Mg–Fe–O phases with higher amount of oxygen compared to specimen pre-oxidized at 900 °C. The number of 316 L grains is significantly lower than respective amount for 900 °C pre-oxidized specimen, clusters of such grains are surrounded by oxides of Fe and Mg, contributing to the non-conductive behavior of the 1000 °C specimens (Fig. 16).

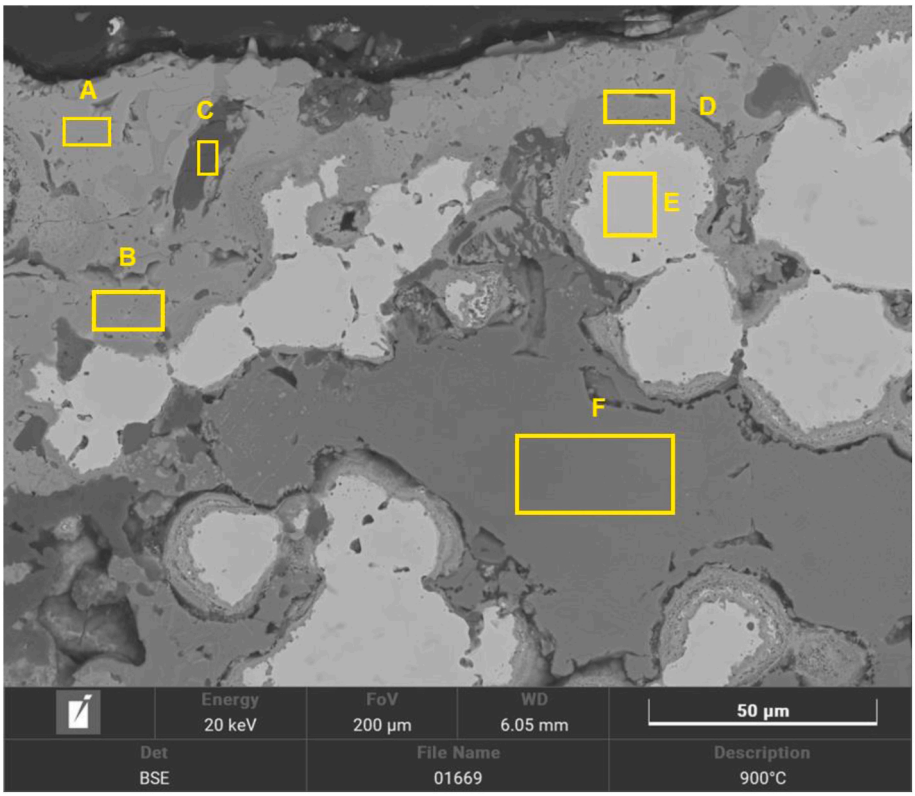

Fig. 17. REM/EDS analysis (BSE mode) of the surface of the specimen pre-oxidized at 900 °C.

In order to evaluate newly formed phases on the specimen pre-oxidized at 900 °C, showing better results in electrical conductivity and mechanical properties, REM/EDS analysis was conducted (Fig. 17).

Brighter area A, mostly exposed to the surface oxidation contains mostly FeO phases. Slightly darker areas B and D are almost identical, with solid solution of MgO and FeO phases, with higher amount of the latter. Area E represents 316 L stainless steel grain, area C is the remaining part of not-reacted MgO grains. Area F is a solid solution of FeO and MgO phases, with a higher amount of MgO. Alloying elements of steel and residual elements from recycled MgO are present in all areas. It should be mentioned that the highest content of such alloying elements is present in area F surrounding 316 L grains, forming complex Fe–Mg–Si–Ca–Mn–Cr–O transition phases.

4. Conclusion

Recycled MgO–C lining bricks after burnout of the carbon can be utilized to produce inert anodes based on metal-ceramic composite with 60 vol% of 316 L stainless steel and 40 vol% of recycled MgO material. In order to manufacture comparatively large parts with a low shrinkage, additional step of granulation and sintering of the fine powders has to be performed. Such step decreases shrinkage caused by sintering from around 4% for fine powders down to 0.75% in length direction for mixture of fine-powders (40 wt%) with pre-sintered granulates (60 wt %).

The developed composite material forms protective layer during the pre-oxidation thermal treatment. Such protective layer mostly contains FeO–MgO solid solution phases. The evaluation of the mechanical tests as well as electrical conductivity measurement showed that the most suitable pre-oxidation temperature for the material studied is 900 °C. Anodes pre-oxidized at 900 °C exhibited electrical conductivity of 150 S/cm at the room temperature, comparable with inert anodes for aluminium-cryolite electrolytic cells. Since the newly formed oxide phases are semi-conductive while the metal matrix composite inside is electrically conductive, it is assumed that with increasing temperatures the overall conductivity of the composite system will decrease less compared to graphite.

In the further studies, electrical conductivity tests at elevated temperatures and electro-chemical analysis after the corrosion tests will be performed.

Declaration of interests

The authors declare that they have no known competing financial interests or personal relationships that could have appeared to influence the work reported in this paper.

Funding

This research was funded by the German Research Foundation (DFG), Germany, project number GRK2802 461482547.

Author agreement

All authors have seen and agree with the contents of the manuscript and confirm that the submission is not under review at any other publication. All other agree to the submission/publication of the manuscript in Open Ceramics.

Acknowledgements

The authors would like to thank G. Schmidt and C. Ludewig for help with calorimetry and microscopical analysis as well as R. Fricke and R. Kaulfürst for technical support.

References

[1] L. Horckmans, P. Nielsen, P. Dierckx, A. Ducastel, Recycling of refractory bricks used in basic steelmaking: a review, Resour. Conserv. Recycl. 140 (2019) 297–304.

[2] L. McDonald, Fostering sustainability in the refractories industry, Am. Ceram. Soc. Bull. 101 (2022) 36–37.
[3] N. Bannenberg, K.J. Arlt, Utilisation of Used Refractory Material and Slag as Secondary Raw Materials, 1997, pp. 3–10.
[4] Z. Liu, J. Yu, X. Wang, P. Ma, W. Gu, J. Wen, S. Wei, X. Zhang, Z. Yan, T. Wen, L. Yuan, B. Ma, Comparative study of B_4C, $Mg_2B_2O_5$, and ZrB_2 powder additions on the mechanical properties, oxidation, and slag corrosion resistance of MgO–C refractories, Ceram. Int. 48 (10) (2022) 14117–14126.
[5] Q. Gu, T. Ma, F. Zhao, Q. Jia, X. Liu, G. Liu, H. Li, Enhancement of the thermal shock resistance of MgO–C slide plate materials with the addition of nano-ZrO_2 modified magnesia aggregates, J. Alloys Compd. 847 (2020), 156339.
[6] Q. Gu, F. Zhao, X. Liu, Q. Jia, Preparation and thermal shock behavior of nanoscale MgAl2O4 spinel-toughened MgO-based refractory aggregates, Ceram. Int. 45 (9) (2019) 12093–12100.
[7] J. Xiao, J. Chen, Y. Wei, Y. Zhang, S. Zhang, N. Lim, Oxidation behaviors of MgO-C refractories with different Si/SiC ratio in the 1100–1500 °C range, Ceram. Int. 45 (17A) (2019) 21099–21107.
[8] G. Klages, H. Naefe, R. Solmecke, E. Thiemann, Environmental aspects in the application of refractories for converter linings in Germany, in: Proceedings of the 1. European Oxygen Steelmaking Congress, Düsseldorf/Neuss, Germany, 21–23 June 1993, pp. 254–259.
[9] K. Moritz, N. Brachhold, J. Hubálková, G. Schmidt, C.G. Aneziris, Utilization of recycled material for producing magnesia–carbon refractories, Ceramics 6 (1) (2023) 30–42, https://doi.org/10.3390/ceramics6010003.
[10] H.M. Oh, Y.J. Park, H.N. Kim, et al., Remarkable plasma-resistance performance by nanocrystalline Y_2O_3·MgO composite ceramics for semiconductor industry applications, Sci. Rep. 11 (2021), 10288, https://doi.org/10.1038/s41598-021-89664-9.
[11] P. Malczyk, T. Zienert, F. Kerber, C. Weigelt, S.-O. Sauke, H. Semrau, G. Aneziris C, Corrosion-resistant steel–MgO composites as refractory materials for molten aluminum alloys, Materials 13 (21) (2020) 4737, https://doi.org/10.3390/ma13214737.
[12] O. Fabrichnaya, The assessment of thermodynamic parameters for solid phases in the Fe-Mg-O and Fe-Mg-Si-O systems, Calphad 22 (1) (1998) 85–125.
[13] C. Weigelt, S. Yaroshevskyi, F. Kerber, N. Brachhold, T. Zienert, A. Adamczyk, D. Vogt, A. Charitos, C.G. Aneziris, Investigations on the Corrosion of 316L Steel Composite Materials with MgO/TiO2 Ceramic Immersed in Molten Cryolite, Open Ceram (2023) 15.
[14] J.S. Haggerty, D.R. Sadoway, Investigation of Materials for Inert Electrodes in Aluminum Electrodeposition Cells, United States, 1987, https://doi.org/10.2172/5743785.
[15] Awayssa Omar, et al., Electrochemical production of Al-Si alloys in cryolitic melts in a laboratory cell, J. Electrochem. (2021), https://doi.org/10.1149/1945-7111/abf40e. Soc. **168** 046506.
[16] I. Galasiu, R. Galasiu, C. Nicolescu, J. Thonstad, G.M. Haarberg, The behaviour of phosphorus and sulfur in cryolite-alumina melts: thermodynamic considerations, in: M. Gaune-Escard, K.R. Seddon (Eds.), Molten Salts and Ionic Liquids, 2010, https://doi.org/10.1002/9780470947777.ch10.
[17] A.S. Yasinskiy, S.K. Padamata, P.V. Polyakov, A.V. Shabanov, An update on inert anodes for aluminium electrolysis, Non Ferr. Met 48 (2020) 15–23.
[18] Asbjørn, S. Inert Anodes—the Blind Alley to Environmental Friendliness? In: Martin, O. (eds) Light Metals 2018. TMS 2018. The Minerals, Metals & Materials Series. Springer, Cham. https://doi.org/10.1007/978-3-319-72284-9_164..
[19] Y.F. Kargin, E.N. Samoilov, V.I. Makarenkov, et al., Metal-ceramic composites based on iron oxide for low-consumption anode during electrolytic extraction of aluminum, Inorg. Mater. Appl. Res. 9 (2018) 52–56, https://doi.org/10.1134/S207511331801015X.
[20] W. Li, G. Zhang, J. Li, et al., NiFe2O4-based cermet inert anodes for aluminum electrolysis, JOM (J. Occup. Med.) 61 (2009) 39–43, https://doi.org/10.1007/s11837-009-0068-9.
[21] Y. Liu, Y. Zhang, W. Wang, D. Li, J. Ma, Microstructure and electrolysis behavior of self-healing Cu – Ni – Fe composite inert anodes for aluminum electrowinning. International journal of minerals, Metallurgy and Mater. 25 (10) (2018) 1208–1216.
[22] T. Zienert, M. Farhani, S. Dudczig, C.G. Aneziris, Coarse-grained refractory composites based on Nb-Al_2O_3 and Ta-Al_2O_3 castables, Ceram. Int. 44 (2018) 16809–16818.
[23] T. Zienert, D. Endler, J. Hubálková, G. Günay, A. Weidner, H. Biermann, B. Kraft, S. Wagner, C.G. Aneziris, Synthesis of niobium-alumina composite aggregates and their application in coarse-grained refractory ceramic-metal castables, Materials 14 (21) (2021) 6453, https://doi.org/10.3390/ma14216453.
[24] G. Routschka, H. Wuthnow, Handbook of Refractory Materials, fourth ed., Vulkan-Verlag GmbH, 2012.
[25] Hanspeter Alder, United States Patent, US3960678, 1976.
[26] G.M. Haarberg, "The interaction between tin oxide and cryolite-alumina melts, in: 9th Int. Symp. On Molten Salts. San Francisco, USA, 22-27 May 1994, Molten Salts, Electrochemical Society, Inc, 1994, pp. 568–577.
[27] S.P. Ray, R.A. Rapp, United States Patent, US4454015, 1984.
[28] S.P. Ray, R.A. Rapp, United States Patent, US4584172, 1986.
[29] S.K. Padamata, A. Yasinskiy, P. Polyakov, Progress of inert anodes in aluminium industry: review, J. Siberian Federal Univ. Chem. (2018 11), https://doi.org/10.17516/1998-2836-0055.